POLITECNICO DI TORINO
Repository ISTITUZIONALE

Coherent and Spectral Beam Combining Approaches to Lunar Wireless Power Transmission

Original
Coherent and Spectral Beam Combining Approaches to Lunar Wireless Power Transmission / Mauro, A., Mauro, S., Perrone, G.. - ELETTRONICO. - (2025), pp. 145-159. (INTERNATIONAL ASTRONAUTICAL CONGRESS Sydney (Aus) 29 September - 3 October 2025) [10.52202/083089-0015].

Availability:
This version is available at: 11583/3007103 since: 2026-01-29T21:57:48Z

Publisher:
International Astronautical Federation (IAF)

Published
DOI:10.52202/083089-0015

Terms of use:

This article is made available under terms and conditions as specified in the corresponding bibliographic description in the repository

Publisher copyright

(Article begins on next page)

27 November 2026

76th International Astronautical Congress (IAC) 2025 - Sydney, Australia
Copyright 2025 by the authors, Published by the IAF, with permission and released to the IAF to publish in all forms.

IAC-25,C3,2,4,x98663

Coherent and spectral beam combining approaches to Lunar wireless power transmission

Anna Mauro[1,2,*], Stefano Mauro[3], and Guido Perrone[1]

[1] *Department of Electronics and Telecommunications, Politecnico di Torino, 10129, Torino, Italy*

[2] *ORIS, Turin, Italy*

[3] *Department of Mechanical & Aerospace Engineering, Politecnico di Torino, 10129, Torino, Italy*

[*]Corresponding author
Email: anna.mauro@polito.it

Abstract

Future lunar missions require reliable energy sources to support intensive surface operations and activities including robotic and human exploration, in-situ resource utilization, and scientific activities. Continuous power availability is a challenge, particularly in permanently shadowed regions and during the lunar night. Space-based wireless power transmission (WPT) can be a transformative technology for enabling sustainable lunar exploration and habitation. This study explores coherent and spectral beam combining (CBC and SBC) approaches for high-power laser-based WPT onboard a satellite constellation designed to provide continuous energy to the lunar surface. The research is part of the all-italian DESIGN project funded by the Italian Space Agency (ASI) in the context of development of projects and scientific experiments for the Moon. Laser-based WPT systems must overcome significant challenges, including working reliably in a space environment, delivery over very long distances, and power scalability. Coherent and spectral beam combining techniques offer promising solutions to enhance power delivery by mitigating diffraction limitations and improving thermal management. CBC achieves high-intensity beams through phase control of multiple laser sources, while SBC increases total transmitted power by combining different wavelength channels. Both methods have been extensively studied for terrestrial applications, but their implementation in space environments requires new design considerations. This first phase of the project focuses on modeling and simulating CBC and SBC architectures in the space context, evaluating their performance in terms of power density, pointing accuracy, and resilience to space-induced perturbations. The study will assess key technological trade-offs, including laser array configurations, phase stabilization mechanisms, and optical receiver designs for maximum energy conversion efficiency on the lunar surface. The findings of this research will inform the development of a prototype system for future experimental validation and contribute to the broader vision of sustainable lunar infrastructure. The outcomes will also have implications for deep-space applications, including planetary exploration and space-based solar power systems.

1. Introduction

1.1 Motivation: continuous lunar power as a key enabler for long-term missions

Sustained exploration of the Moon requires reliable and continuous sources of energy to support both robotic and human activities. Power is needed not only for life support and scientific instruments, but also for mobility systems, in-situ resource utilisation, and future construction of permanent infrastructure. Unlike low-Earth orbit platforms, which benefit from frequent sunlight and short eclipse durations, lunar surface operations face far harsher conditions. One of the most significant challenges is the long lunar night, which lasts approximately fourteen Earth days. During this period, surface temperatures drop drastically and solar photovoltaic systems become unusable without large, heavy energy storage. Similarly, permanently shadowed regions at the poles, which

Copyright 2025 by the authors, Published by the IAF, with permission and released to the IAF to publish in all forms.

are of high scientific and resource interest, never receive direct sunlight. These environments cannot be supported by conventional solar-only architectures. Infrastructure limitations further compound the problem. Transporting large batteries, nuclear sources, or kilometre-scale solar farms to the Moon remains impractical in the near term due to mass and deployment constraints. As a result, continuous and flexible power delivery methods are a critical missing element for enabling long-duration missions and sustained habitation. Wireless power transmission (WPT) from space-based platforms offers a transformative solution: satellites in appropriate orbits can provide uninterrupted energy beams to selected surface sites, bypassing the day–night cycle and shadowing effects. This capability is a cornerstone for building resilient lunar infrastructure and supporting the vision of a permanent human and robotic presence.

1.2 Wireless Power Transmission as a solution

Wireless power transmission (WPT) offers a means to overcome the inherent limitations of traditional solar-based architectures on the lunar surface. By placing high-power laser transmitters on satellites in polar orbits or halo orbits around the Moon, energy can be delivered continuously to surface receivers, independent of local lighting conditions. The concept decouples energy availability from the lunar day/night cycle and enables access to permanently shadowed regions, where valuable volatiles and scientific opportunities exist but conventional solar arrays are ineffective. Laser-based WPT is particularly attractive because it combines high directionality with modular scalability: multiple laser channels can be combined to reach the required power levels, and lightweight photonic power converters (PPCs) can be deployed on the surface to capture and transform the optical beam into usable electrical power. This approach reduces the need for massive batteries, nuclear reactors, or large-scale solar farms, thereby lowering launch mass and deployment complexity for each lunar mission. WPT thus represents a promising enabling technology for continuous operations, long-duration habitation, and the establishment of sustainable lunar infrastructure.

2. Background

2.1 WPT Overview (microwave,laser..)

High-power laser systems suitable for wireless power transmission cannot be realised from a single fiber amplifier channel, because individual fibers are limited in their maximum output by nonlinear effects, thermal constraints, and damage thresholds. To reach the multi-kilowatt to megawatt power levels needed for lunar applications, we investigate the combination of multiple channels. Two main approaches have emerged for this purpose: coherent beam combining (CBC) and spectral beam combining (SBC). In CBC, as the name suggests, the *coherence* among the output beams from many emitters that share the same wavelength and are actively phase-locked, so that their optical fields interfere constructively and form a diffraction-limited far-field beam. In SBC, each emitter operates at a slightly different wavelength, and the channels are superimposed coaxially using wavelength-selective optics; their fields do not interfere but their intensities add, producing a broadband beam whose total power scales with the number of channels. Both methods have been extensively demonstrated in terrestrial fiber laser research and are regarded as the most viable paths for scaling laser power to the levels required in space-based wireless power transmission [1].

2.2 CBC and SBC: definitions, pros & cons

Coherent beam combination is a technique that combines high-power laser beams to obtain a single output beam with preserved beam quality, increased brightness, and increased power. The beams are combined because the output of a single laser is limited by the power density it can handle, by nonlinear effects, e.g. stimulated Raman scattering (SRS) in the case of fiber lasers. Combining multple beams to increase the power of continuous lasers allows to design higher power, high quality lasers while avoiding these limitations [2], [3]. Spectral beam combination, in contrast, does not rely on maintaining a fixed phase relationship between emitters. Instead, individual lasers are operated at slightly different wave-

Copyright 2025 by the authors, Published by the IAF, with permission and released to the IAF to publish in all forms.

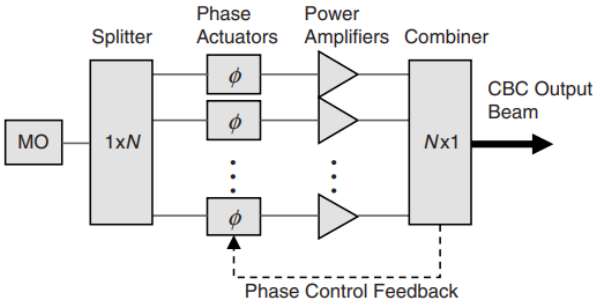

Figure 1: *We assume the beams are derived from a common master oscillator (MO), assumed to be quasi-monochromatic with carrier frequency ω_0 and time-varying modulated phase $\varphi(t)$*

lengths and are combined using wavelength-selective optics such as diffraction gratings or dichroic mirrors. Since each channel is independent in phase, the total output intensity is simply the sum of the intensities of the individual beams, with no requirement for interferometric stability. This approach enables straightforward power scaling and avoids the complexity of phase control loops, but it does not preserve diffraction-limited beam quality in the same sense as coherent beam combining. Rather, the combined beam quality depends on the spectral spacing of the channels and the properties of the combining optics. While spectral combining therefore results in a lower brightness increase compared to coherent combining, it offers a more robust and mechanically simpler architecture, particularly advantageous in environments where vibration or thermal perturbations can disrupt phase locking [4], [5], [6]. In the lunar context, coherent and spectral beam combining present complementary strengths and limitations, summarized in Table 1. CBC offers the ability to form a near-diffraction-limited spot at the receiver, which maximises the power density and allows for compact photovoltaic converters. However, this benefit comes at the cost of significant complexity: phase control requires nanometre-level path length stability, which is difficult to guarantee on a spacecraft subject to thermal and vibrational disturbances [7]. SBC, by contrast, eliminates the need for phase coherence. Each MOPA channel operates independently at a distinct wavelength and is superimposed by dichroics or gratings, making the architecture inherently modular and more robust against mechanical perturbations. The trade-off is that the resulting beam has a broader far-field profile, reducing the peak intensity at the receiver and increasing the required aperture area for efficient energy collection. In summary, CBC is best suited to applications where maximising intensity on a small receiver is essential, whereas SBC favours scalability, fault tolerance, and simplified operations in a space environment.

CBC of multiple lasers can only be achieved if all the laser beams are mutually coherent, which requires the same optical properties such as polarization state and spatial mode structure for all the laser beams. This mutual coherence can be realized, for example, by splitting a single laser beam (seed laser) via fiber couplers or optical coupling synchronization with multicore fibers. Active phase-locking systems consist of two parts: phase detection and active phase noise correction. The latter is usually implemented with electro-optical modulators, liquid crystal modulators, and piezo-electric actuators. Hill climbing is the simplest method for active phase-locking of multiple laser beams, in which the cophasing is achieved by maximizing the combined laser power in the far-field central lobe. In this case, no phase detection is needed, and the stochastic parallel gradient descent (SPGD) optimization algorithm is utilized to maximize the combined power [8],[9]. This technique requires a single detector to obtain the required feedback, simplifying the operation. The number of intensity measurements can therefore remain constant regardless of N. Computing the update, however, still involves on the order of N operations to adjust each channel's phase (but this scaling is modest). However, the *convergence time* of SPGD tends to increase with the dimensionality of the problem, since in practice larger arrays require more iterations for phase-locking and can exhibit slower convergence [10]. A long-standing problem in CBC is that the effective *control bandwidth* decreases as the number of lasers increases [11]. As N grows, SPGD controllers have to work harder to maintain lock, resulting in a narrower feedback bandwidth for phase noise correction. For example, one FPGA-based SPGD controller achieved a ~1.9 MHz iteration rate, yielding a ~50 kHz phase compensation bandwidth for a

Copyright 2025 by the authors, Published by the IAF, with permission and released to the IAF to publish in all forms.

Aspect	CBC (Coherent Beam Combining)	SBC (Spectral Beam Combining)
Beam Quality	Very high: diffraction-limited central lobe	Very high: each wavelength propagates independently with diffraction-limited quality
Power Scaling	Limited by phase control complexity and coherence length	Excellent: power scales linearly with number of channels, no coherence requirement
Control Requirements	Active phase stabilisation and wavefront sensing essential	Only wavelength alignment and beam pointing needed
Sensitivity to Vibrations / Thermal Drift	nm-level path fluctuations cause phase noise and degrade performance	Channels are independent, phase is irrelevant
System Modularity	Channels are phase-coupled and must be synchronised	Each module is independent, easier to swap/replace
Complexity	Requires feedback loops, feedback control	Requires dichroic/grating free-space optics, but no phase locking
Efficiency	Very high if phase locked; losses increase rapidly with noise	Slightly lower due to combining optics, but robust to environment
Technology Maturity (for space)	Most CBC systems at TRL 4–5 for space	SBC components (dichroics, gratings, MOPA modules) between TRL 6 to 9
Robustness	Fragile to phase errors, vibration, thermal drift	Robust to phase noise, more fault-tolerant
Receiver Design	Concentrated high-brightness spot could enable smaller, lighter PV receiver	Larger spot leads to lower intensity, requires larger PV area or more sensitive converter
Operation in Lunar Context	When high concentration on a small target is required, and when mechanical movements are inhibited (e.g. powering a rover or ISRU unit with limited aperture, in a dusty lunar environment)	When scalability and robustness are key (e.g. continuous power from satellite constellation, less critical spot size)

Table 1: *CBC vs SBC methods for Lunar Laser WPT.*

5-channel fiber laser array – but the same system could only achieve Ĩ2.5 kHz bandwidth for a 20-channel array. This illustrates how scaling to tens of channels can push the control loop toward slower response. With scaling of the number of lasers, combining efficiency degrades because of system errors and limited control bandwidth, algorithmic enhancements must be introduced to maintain performance [12]. Real time implementation can have several practical limitations - fast phase disturbances, such as high-frequency mechanical vibrations or rapid thermal fluctuations might not be fully corrected if they lie outside the controller's bandwidth. Without enhancements, the system may fail to maintain coher-

Copyright 2025 by the authors, Published by the IAF, with permission and released to the IAF to publish in all forms.

ent combining under fast dynamics once N is high. The stochastic nature means the beam quality will exhibit some residual jitter as phases are continually dithered. In a targeting system, this residual error must be quantified to ensure it meets requirements, e.g. pointing stability. Latency between applying a perturbation and measuring the result (due to finite optical propagation or electronics delay) can corrupt the gradient estimate, for which a time delay should be optimized to ensure the perturbations are measured correctly. Fortunately, SPGD algorithms implemented in FPGA logic can be made quite power-efficient relative to, say, running equivalent code on a general CPU, but the total system (including high-speed ADCs, DACs, and phase modulators) will draw noticeable power that needs budgeting in a satellite. These factors don't negate SPGD's viability, but they impose engineering limits on how the system is designed and operated.

2.3 Key differences in space-based implementation

At the present state, microvibrations in spacecraft cannot be actively controlled because their very high frequencies of up to 1000 Hz are above the control bandwidth a current attitude control system can provide [13]. Sampling rate of various MEMS accelerometers can go up to 4 kHz, sufficient to measure vibrations of half this frequency. Achieving real-time phase control at MHz-scale update rates for tens of channels is a significant computing challenge. In this work, we assume that the highest jitter frequency of the platform is 1 kHz (so sampling rate $f_s > 2$ kHz), while the control bandwidth is 150 Hz. Therefore, 150-1000 Hz disturbances go by uncorrected, directly hitting the array phases. An update rate on the order of 10^6 iterations per second implies sub-microsecond processing per iteration, including applying perturbations to 10–100 phase modulators, reading the sensor, and computing the next update. This phase controller can be made by a field programmable gate array (FPGA) to implement the algorithm, since they offer highly parallel, deterministic processing with low latency [14]. Chang et al. (2020) [12] built a 107-channel fiber laser CBC system using an FPGA-based SPGD controller, achieving an execution frequency over 1 MHz (i.e. $> 10^6$ updates per second) to track high-frequency phase noise. For space-based implementation, radiation-tolerant or -hardened FPGAs would be the primary choice. These can be clocked at hundreds of MHz and configured with dedicated parallel pipelines for each channel. This allows for all 10-100 phase updates and the gradient calculation to be executed concurrently each cycle.

3. System concept, Mission scenario

The proposed system aims to provide a robust and scalable solution for wireless power transmission (WPT) from lunar orbit to the surface. The primary objective of this architecture is to address the critical energy requirements of future lunar bases, supporting both human activities and autonomous operations, including exploration, in-situ resource utilization (ISRU), and life-support systems. Ensuring a continuous and reliable power supply on the lunar surface presents unique challenges due to the Moon's long night cycles, extreme temperature variations, and terrain-induced shadowing, particularly at the South Pole where permanently shadowed regions (PSRs) are located. Traditional solar power generation is highly limited under these conditions, motivating the development of orbital power relay systems capable of delivering energy regardless of local illumination. The ORiS concept leverages a constellation of satellites in lunar orbit, each equipped with high-efficiency photovoltaic arrays and fiber-based high-power laser sources. These satellites collect solar energy and convert it into coherent or spectrally combined laser beams, which are then precisely directed toward ground-based receivers. The combination of orbital mobility and optical power transmission enables continuous energy delivery to targeted locations on the surface, regardless of local sunlight availability. This system concept not only addresses the immediate energy needs of lunar outposts but also provides flexibility for mission planners. By varying the orbital configuration, the number of satellites, and the laser transmission strategies, the architecture can be tailored to meet specific site requirements, whether for polar research stations, equatorial habitats, or mobile assets such as rovers and drones. Fur-

Copyright 2025 by the authors, Published by the IAF, with permission and released to the IAF to publish in all forms.

thermore, the modular design of both satellites and ground receivers ensures scalability, fault tolerance, and redundancy, enhancing the overall reliability of the system. In this section, we provide a comprehensive overview of the mission scenario, including the orbital constellation, surface power requirements, key system assumptions, and a high-level depiction of the architecture. Special emphasis is placed on the integration of advanced photonic technologies for energy conversion and the management of operational constraints imposed by the lunar environment.

3.1 Description of orbital constellation (altitude, orbits, coverage,..)

The proposed orbital constellation consists of multiple satellites designed to collect solar energy and deliver it to the lunar surface via high-power laser beams. Each satellite integrates photovoltaic arrays, energy storage, and fiber-based laser transmitters, forming a modular and autonomous unit capable of continuous operation in lunar orbit. Three orbital configurations have been analyzed to evaluate coverage, transmission time, and overall energy delivery efficiency:

- **Circular Polar Lunar Orbit:** Satellites at an altitude of 600 [km] with an inclination of $89.54°$, aimed at high-latitude regions such as the Shackleton crater. This orbit maximizes coverage of polar areas but requires frequent station-keeping due to gravitational perturbations.
- **Low Elliptical Lunar Frozen Orbit:** Average altitude of 100 [km], with parameters $a = 1838$ [km], $e = 0.01$, $i = 88°$, $\omega = 270°$, RAAN $= 0°$. This orbit reduces natural orbital drift, offering higher stability, but the shorter dwell time within the transmission cone limits the average transmitted power.
- **Distant Retrograde Orbit (DRO):** Average altitude of 800 [km], neutrally stable in the Earth-Moon system, modeled using the Circular Restricted Three-Body Problem (CR3BP). This configuration maximizes coverage duration for equatorial receivers, allowing longer continuous transmission periods and higher energy delivery.

Energy transmission occurs only when satellites are within the defined *transmission cone*, characterized by a maximum angle θ_{max} between the satellite and the ground receiver. Various cone angles $(50°, 60°, 70°, 80°)$ have been analyzed. For example, in a 600 [km] circular polar orbit with $\theta_{\text{max}} = 60°$, a satellite remains within the transmission cone for approximately 1,123 s (18 minutes and 43 seconds). The effective received power per satellite can be expressed as:

$$P_r = P_L \cdot \eta_L \cdot \eta_{\text{cell}}, \tag{1}$$

where $P_L = 30$ [kW] is the laser output power, $\eta_L = 50\%$ the laser efficiency, and $\eta_{\text{cell}} = 68.9\%$ the photonic power converter efficiency. This yields $P_r \approx 10.34$ [kW]. In the most favorable scenario (DRO, 10 satellites, $\theta_{\text{max}} = 80°$), the constellation can provide roughly 519 [kWh] per lunar day, covering approximately 20% of the energy requirements of a medium-scale lunar outpost. This constellation design offers flexibility in terms of coverage, transmission timing, and scalability, ensuring that energy can be delivered to key lunar sites independently of local illumination conditions.

3.2 Surface Operations and Power Needs (Day/Night, ISRU)

The primary objective of the proposed system is to provide reliable energy to critical lunar surface operations, particularly at high-priority sites such as the South Pole (e.g., Shackleton crater) and equatorial regions. Lunar surface activities include human habitats, robotic exploration, and in-situ resource utilization (ISRU), all of which impose distinct and sometimes peak power demands. One of the key challenges is the lunar environment itself. The Moon experiences extremely long nights, approximately 14 Earth days each, during which solar power generation is not feasible. Additionally, topographic features such as deep craters and high mountains create permanently shadowed regions (PSRs) that further limit local solar illumination. These factors necessitate a continuous, non-solar-dependent power supply. The energy requirements of a typical lunar outpost are estimated as follows:

- **ISRU operations:** Extraction and transporta-

Copyright 2025 by the authors, Published by the IAF, with permission and released to the IAF to publish in all forms.

tion of lunar resources require 60–100 [kW].

- **Human habitats:** Life support, thermal regulation, and operational equipment for a crew of four require 20–50 [kW].
- **Rovers and drones:** Autonomous vehicles for exploration and logistics consume up to $\sim$500 [W] per unit.

Surface receivers, referred to as *Photonic Power Converters (PPCs)*, convert the incoming laser energy into electricity. These receivers are designed to optimize conversion efficiency under monochromatic laser illumination. Key characteristics include:

- **Conversion Efficiency:** Laboratory-tested efficiencies up to 68.9% for GaAs-based cells under 1064 nm laser illumination.
- **Material Selection:** GaAs, InGaAs, and InAlGaAs cells are suitable for the selected laser wavelength, offering high performance for both high-power density and long-duration exposure.
- **Receiver Geometry:** The PPC array is optimized to minimize cosine losses and maximize effective area, with a typical configuration of 99$\times$99 cells. The effective receiving area ranges from 34.9 [m^2] ($\theta_{\text{max}} = 50°$) to 54.1 [m^2] ($\theta_{\text{max}} = 80°$), ensuring sufficient energy capture across varying beam incidence angles.

By matching the design of orbital transmitters with appropriately sized and positioned PPCs on the lunar surface, the system can ensure a continuous and sufficient power supply for both human and robotic operations, independent of local sunlight availability. This approach is particularly critical for maintaining operations in PSRs and during the lunar night, where conventional solar panels would be ineffective.

3.3 Scenario Assumptions

To define a consistent framework for analyzing lunar power transmission, several key assumptions have been adopted regarding the laser system, optical propagation, and spacecraft pointing capabilities.

3.3.1 Laser System Parameters:

Each satellite is equipped with high-power fiber lasers doped with ytterbium, selected for their high beam quality, electrical-to-optical efficiency, and robustness in space. The nominal laser output power is set at $P_L = 30$ [kW], with an electro-optical efficiency of $\eta_L = 50\%$. The emission wavelength is $\lambda = 1064$ nm, chosen for compatibility with high-efficiency photonic power converters and for minimal atmospheric absorption in a near-vacuum environment.

3.3.2 Beam Collimation and Quality:

The laser beams are expanded and collimated using off-axis metallic parabolic mirrors, which facilitate thermal management and maintain high optical performance over long distances. The beam waist is fixed at $w_0 = 250$ mm, and the beam quality factor is $M^2 = 11.8$, which sets limits on achievable spot size and power density at the lunar surface.

3.3.3 Spacecraft Pointing and Attitude Control:

Precise pointing is critical to maintain energy delivery efficiency. The system assumes a pointing accuracy on the order of a tenth of an arcsecond. A three-level pointing strategy is adopted:

1. **Satellite GNC (Guidance, Navigation, and Control):** Maintains coarse attitude and orbital stability.
2. **Two-Axis Gimbal:** Provides intermediate pointing adjustments, compensating for larger orbital and thermal perturbations.
3. **Fine Steering Mirrors (FSM):** High-speed piezoelectric actuators correct residual pointing errors, ensuring the beam remains accurately aligned with the surface receiver.

Transmission occurs only when satellites are within the defined transmission cone of the ground receiver, which varies between $50°$ and $80°$ in the analyzed scenarios. The design also assumes negligible atmospheric losses (vacuum environment) and minimal beam divergence outside the inherent diffraction limit. By establishing these assumptions, the analysis provides a realistic baseline for evaluating system

Copyright 2025 by the authors, Published by the IAF, with permission and released to the IAF to publish in all forms.

performance, coverage, and energy delivery, while highlighting the technical requirements for precise laser transmission and stable satellite operation in lunar orbit.

3.4 System Diagram (High-Level)

The ORiS architecture for lunar wireless power transmission (WPT) is designed to provide continuous power to lunar bases despite long nights and permanently shadowed regions. The system transfers energy from orbital solar collection to surface utilization.

Phase A: Energy Collection and Storage (Satellite)

1. Solar Energy Collection: A constellation of 3 to 10 satellites orbits the Moon in stable trajectories, such as frozen orbits or Distant Retrograde Orbits (DROs), each equipped with photovoltaic arrays totaling 22 [m^2]. 2. Energy Storage (EPS): Electrical energy is stored in lithium-ion batteries sized to power the high-power laser (30 [kW]). Batteries are managed to maintain the State of Charge (SoC) between 10% and 90% during orbital cycles. 3. Laser Power Supply: Stored energy feeds the laser payload.

Phase B: Laser Generation and Beam Management (Payload)

4. Optical Generation: High-power ytterbium-doped fiber lasers provide 30 [kW] peak power with 50% electro-optical efficiency at 1064 nm. 5. Beam Expansion and Collimation: The beam is expanded and collimated using off-axis metallic parabolic mirrors to maintain a reasonable diameter on the lunar surface over hundreds of kilometers.

Phase C: Transmission and Pointing (Free Space)

6. Precision Pointing: A three-level system compensates for vibrations and orbital disturbances: satellite GNC, two-axis gimbal, and fine steering mirrors (FSM) with piezoelectric actuators. 7. Laser Transmission: The collimated beam propagates through vacuum, where diffraction dominates, and is transmitted only within the defined transmission cone (α_{max}).

Phase D: Reception and Conversion (Lunar Surface)

8. Receivers (PPCs): Photonic Power Converters capture optical energy with a modeled conversion efficiency of 68.9% using GaAs-based cells. Materials like InGaAs are considered for 1064 nm. 9. Receiver Structure: Optimized with a base radius of 3 [m] to minimize cosine losses and allow multiple beams reception. 10. End Use: Converted electrical power is stored in surface batteries or used immediately to supply infrastructure, habitats, rovers, and ISRU operations.

The ORiS system establishes an optical energy bridge decoupling generation from usage, providing reliable and scalable electrical power regardless of extreme surface illumination conditions.

3.5 CBC and SBC architectures

The Coherent Beam Combining (CBC) architecture is based on a tiled-aperture laser array arranged on a compact hexagonal 2D shape, as shown in figure 2 [15]. Each element of the array consists of a master-oscillator power-amplifier (MOPA) channel, comprising a narrow-linewidth seed laser, preamplifier stages, and a high-power ytterbium-doped fiber amplifier. The output of each channel is collimated and directed into free space by a dedicated collimator lens, forming one aperture element of the array. The hexagonal packing of these emitters maximises the filling factor and optical aperture efficiency, providing a nearly circular overall beam footprint while maintaining modularity of the individual laser units. To achieve coherent addition, each channel includes a phase control element—typically a fiber stretcher or electro-optic phase modulator—that adjusts the optical path length under feedback control. The array is mounted on a rigid optical bench to preserve relative alignment, with sensors monitoring the combined far-field intensity to provide the feedback signal for phase stabilisation. In operation, the CBC system functions as a synthetic large-aperture laser, where precise phase alignment across the hexagonal array enables the individual beams to interfere constructively, producing a narrow, high-intensity far-field beam suitable for long-distance power transmission. The spectral beam combining (SBC) system is likewise based on a modular array of high-power

Copyright 2025 by the authors, Published by the IAF, with permission and released to the IAF to publish in all forms.

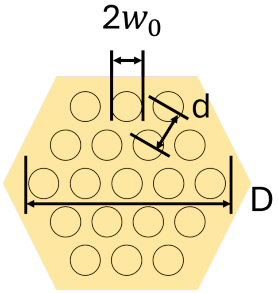

Figure 2: *Hexagonal array geometry, where w_0 is the radius of the single emitter, d is the array pitch, and D is the total diameter of the array.*

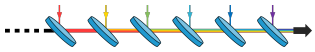

Figure 3: *Spectral Combining stage, where six lasers of different wavelengths (colors) are superimposed to make the combined beam, on the right.*

MOPA channels, each delivering laser output at a distinct wavelength within the ytterbium emission band. Unlike CBC, the SBC channels do not require phase coherence, and each operates independently with its own seed source, amplifiers, and collimation optics. The beams are spatially superimposed along a common optical axis using wavelength-selective optics, such as dichroic mirrors as in 3 or volume Bragg gratings, to form a coaxial output. This architecture preserves the modularity of the individual MOPA units, simplifying control and providing natural redundancy, since the loss of a single channel reduces total power but does not compromise the combined beam. The resulting output is a broadband, multi-wavelength beam in which the total transmitted power scales linearly with the number of active channels. Packaging can be arranged in a compact hexagonal layout for efficient thermal management, but the final combining stage produces a single shared optical aperture.

4. Modeling and Simulation Approach

Satellite platform vibrations can introduce time-varying phase errors in a coherent beam combining (CBC) system. Even a rigid platform will experience translational and rotational jitter that translates into phase disturbances for each laser emitter on the platform. If unaddressed, these phase perturbations can degrade the combined beam's quality and pointing stability. In a MATLAB simulation, we can model these vibrations as correlated phase noise applied to each emitter's phase, and study their impact on CBC performance. Rotational jitter is usually more critical for CBC phase alignment, since a small rotation tilts the entire array, creating a **phase gradient** across the emitters.

4.1 Beam combining principles: CBC (interferometric) vs SBC (intensity sum)

The fundamental difference between coherent and spectral beam combining lies in how the individual channels add up in the far field. In coherent beam combining (CBC), all emitters are phase-locked so that their optical fields interfere constructively. The peak intensity at the receiver scales approximately as N^2, where N is the number of channels, since both amplitude and phase add. This makes CBC conceptually similar to operating a single large-aperture laser: diffraction from the overall aperture defines the beam divergence, while any residual phase error reduces the coherent addition efficiency. In spectral beam combining (SBC), by contrast, the emitters operate at distinct wavelengths and are combined coaxially using wavelength-selective optics. The fields are not phase-coherent with one another, so their contributions add as intensities rather than amplitudes. The total power at the receiver therefore scales linearly with N, without the quadratic enhancement in peak intensity. The far-field profile in SBC is dominated by the diffraction of the common output aperture, with a small broadening due to chromatic spread if the spectral band is wide. Thus, CBC can in principle achieve a higher peak irradiance for the same total power and aperture size, while SBC is simpler, more robust, and offers more scalability.

4.2 Propagation modelling: Gaussian propagation in vacuum and the angular spectrum method

The angular spectrum method is a Fourier optics technique used to model the free-space propagation of a wave field over long distances [16]. In this ap-

Copyright 2025 by the authors, Published by the IAF, with permission and released to the IAF to publish in all forms.

proach, the initial complex field distribution in the source plane is decomposed into a 2D *angular spectrum* of plane waves of the same wavelength by applying a two-dimensional Fourier transform to the initial field:

$$A(k_x, k_y) = F\{U(x, y, 0)\} = \\ = \iint_{-\infty}^{\infty} U(x, y, 0) e^{-i(k_x x + k_y y)} dxdy. \quad (2)$$

Each point in the 2D transform is then multiplied by a propagation term which accounts for the phase change that each plane wave undergoes on its propagation to the target plane:

$$A(k_x, k_y, z) = \\ = A(k_x, k_y, 0) \cdot exp(iz\sqrt{k^2 - k_x^2 - k_y^2}), \quad (3)$$

where $k = 2\pi/\lambda$. The propagated field is then reconstructed in the output plane by applying the corresponding phase shifts in the Fourier domain and performing an inverse transform:

$$U(x, y, z) = F^{-1}\{A(k_x, k_y, z)\}. \quad (4)$$

In the present work, the angular spectrum method provides a numerically efficient way to calculate the far-field intensity distribution from multi-emitter arrays and to evaluate the impact of phase errors and platform jitter on the combined beam profile.

4.3 Perturbation modelling: jitter, vibrational phase noise

Accurate performance prediction of beam combining architectures requires modelling the disturbances that degrade beam quality in realistic space conditions. Two main classes of perturbations are considered: rigid-body pointing jitter and high-frequency vibrational phase noise. Rigid-body jitter arises from the satellite's attitude disturbances, such as reaction wheel imbalance or thruster noise. In this case, the entire array tilts as a rigid platform, so the relative phasing between emitters is preserved. To first order, a θ_x and θ_y rotation about the platform's x and y axes, and translational disturbances $\Delta z(t)$ produce a pathlength change for each emitter proportional to its position offset in the array:

$$\Delta\phi_i(t) \approx \frac{2\pi}{\lambda}[\Delta z(t) + x_i\theta_y(t) - y_i\theta_x(t)], \quad (5)$$

The array-wide rms phase caused by these small rotations can be computed as $\sigma^{tilt} = \frac{2\pi}{\lambda}\sqrt{\sigma_{\theta_y}^2 Var(x) + \sigma_{\theta_x}^2 Var(y)}$, where $Var(x)$ and $Var(y)$ are the variances of the emitter coordinates. The effect is a simple displacement of the far-field beam, which manifests as a pointing error at the lunar receiver. While coherence is not degraded, the captured power depends on the receiver aperture size and the pointing error budget, making pointing stability a key requirement for both CBC and SBC. **Vibrational phase noise**, on the other hand, represents internal structural disturbances that introduce differential path length changes between emitters. These cannot be described as a single rigid tilt, but rather as localised or mode-shaped deformations of the optical bench. Unlike rigid-body tilt, which produces a pure pointing error, in the CBC case this disturbance represents relative phase fluctuations between emitters that cannot be tracked by the control loop. This noise was generated as a Gaussian random process with prescribed temporal bandwidth, filtered to exclude low-frequency piston and tilt modes. Spatial correlations across the array were imposed using an exponential covariance model,

$$C_{ij} = \rho e^{-\frac{d_{ij}}{L_c}} + (1 - \rho)\delta_{ij}, \quad (6)$$

where d_{ij} is the distance between emitters i and j, L_c is the correlation length, and ρ the correlation strength. This formulation allows us to capture both global motions (large L_c, high ρ) and independent local jitter (small L_c, low ρ), and provides a model for introducing realistic relative (correlated) phase errors into CBC simulations. In physical terms, the parameters of the covariance model can be directly related to spacecraft vibration modes, as shown in figure 7. A large correlation length with high correlation strength corresponds to low-order structural modes (7c), such as a bending or twisting of the entire optical bench, where all emitters experience nearly the same disturbance. At intermediate values, the behaviour reflects sub-structures, for example a local

Copyright 2025 by the authors, Published by the IAF, with permission and released to the IAF to publish in all forms.

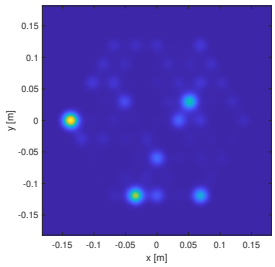

(a) $L_c = 0.05D, \rho = 0.2$. *Local mounts and fibers, high frequency disturbances.*

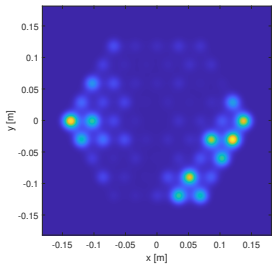

(b) $L_c = 0.5D, \rho = 0.6$. *Substructure modes, mid-frequency bands.*

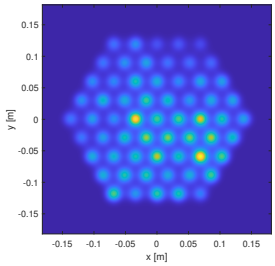

(c) $L_c = 2D, \rho = 0.9$. *Low frequency, global modes.*

Figure 4: *Snapshots of three different regimes of platform disturbances. D is the array diameter [m].*

mounting plate or bracket that deforms over part of the array. At the other extreme, a short correlation length with low strength represents high-frequency, localised jitter where each emitter is affected independently, as might occur with fibre pigtail vibrations or small panel modes. According to [17], for large satellites the first modes can be in the region of e.g. 10 Hz, while around 100 Hz and above can be already referred to as high frequency.

4.3.1 System metrics

The **Strehl ratio** indicates how much peak intensity was lost compared to a perfect, coherent beam:

$$S = \frac{I_{peak,noise}}{I_{peak,ideal}} \tag{7}$$

so $0 < S < 1$. **Power-in-the-bucket** (PIB) is calculated as the fraction of power inside the PV receiver radius at the target plane, over the total power transmitted by the laser:

$$PIB = \frac{P_{received}}{P_{total}} \tag{8}$$

4.4 Optimization of array performance

An optimization of a coherent beam combining (CBC) system for long-distance laser power transmission was carried out. The CBC system consists of an array of Gaussian beams arranged in a hexagonal 2D lattice, with a variable number of concentric rings surrounding a central emitter. The objective was to maximize the *Power-in-the-Bucket* (PIB) at the receiver while ensuring that the overall array diameter does not exceed a predefined maximum, representing optical and mechanical constraints. The optimization explored two parameters: the individual beam waist (w_0) and the inter-element spacing (d), expressed as a multiple of w_0. For each receiver radius, ranging from 1 m to 10 m, the MATLAB framework computed both near-field and far-field intensity distributions. The near field was obtained by superposing the Gaussian profiles of all emitters, while the far field was calculated using Gaussian beam propagation formulas and the *angular spectrum method*, which captures diffraction and interference effects over distances of about 1,200 km. The optimization routine

Copyright 2025 by the authors, Published by the IAF, with permission and released to the IAF to publish in all forms.

is implemented in the `CBCopt` function, which defines a cost function combining two criteria: (i) the deviation of the array diameter from the maximum allowed, and (ii) the fraction of power captured within the receiver aperture. A particle swarm optimization (PSO) algorithm minimizes this cost, yielding the optimal beam waist, inter-element spacing, and resulting array diameter for each receiver configuration. The MATLAB implementation also produces visualizations of near-field and far-field intensity distributions, showing the degree of array coherence and the power fraction collected by the receiver. This methodology provides a systematic evaluation of the trade-offs between array geometry, beam divergence, and receiver aperture in CBC systems.

5. Simulation Results

The propagation results are compared for the two architectures. As explained earlier, the on-board mirror or array diameter affects the diffraction and spot size independently from the laser combining scheme. In system architecture calculations, the dimensions of delivery and reception surfaces (the mirror or array, and the ground receiver) have an important impact on end-to-end system efficiency, being correlated mainly by diffraction and pointing losses. These two surfaces and their design clearly have different mission impacts in terms of cost and deployment. In principle, a receiver that needs to be launched, landed and assembled (either autonomously or manually) on the lunar surface has a bigger impact on these mission drivers rather than a larger diameter mirror onboard a satellite. Therefore, different cases have been studied for receivers of different sizes, and an optimum mirror diameter was calculated in order to maximize end-to-end system efficiency. For consistency across both CBC and SBC architectures, the so-called "power-in-the-bucket" (PIB) efficiency was used in place of the geometric efficiency, as it directly quantifies the fraction of power collected by the receiver. The efficiency is calculated as:

$$\eta_{end-to-end} = \eta_{e-o}\,\eta_{pointing}\,\eta_{o-e}\,\eta_{PIB}\,\eta_{cos} \quad (9)$$

where η_{e-o} is the laser's electro-optical conversion efficiency, $\eta_{pointing}$ is the pointing efficiency (assuming a Gaussian beam), η_{o-e} is the receiver's conversion efficiency, η_{PIB} (power-in-the-bucket) is the fraction of transmitted power collected by the receiver aperture, and η_{cos} is the cosine loss due to the angle between the laser beam and the photovoltaic cells.

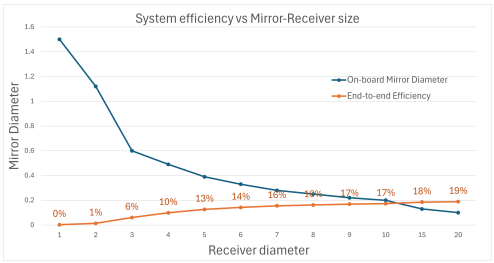

Figure 5: *Optimum laser beam delivery diameter for varying receiver sizes.*

5.1 Beam profile comparisons at lunar distance

The beam profile at the target plane was simulated at maximum transmission distance. The mirror and array apertures were kept constant in both architectures for comparison. Simulations were carried out to propagate the combined beams over a propagation distance of almost 1200 km. The angular spectrum method was used to compute the far-field intensity distribution from the CBC architecture, while the equations for Gaussian propagation in vacuum were used to simulate propagation with a SBC architecture. In the ideal case without phase noise, CBC produced a diffraction-limited central lobe with high contrast, equivalent to that of a single large-aperture emitter. The SBC configuration, with spectrally distinct coaxial beams, yielded a nearly identical envelope, with only minor chromatic broadening. These results confirm that the dominant factor determining beam spread at lunar distance is the physical aperture size rather than the combining method, and that both approaches are able to deliver a well-confined beam to the lunar surface when properly scaled.

5.2 Performance degradation results

The simulation results highlight the differing sensitivity of coherent beam combining to vibration-induced phase noise under various spatial correlation regimes.

Copyright 2025 by the authors, Published by the IAF, with permission and released to the IAF to publish in all forms.

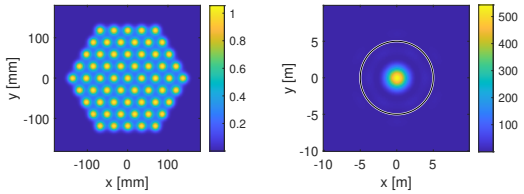

Figure 6: *Near-field and far-field Intensity pattern I(z)*

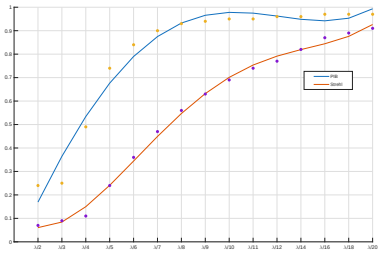

(a) $L_c = 0.05D, \rho = 0.2$. *Local mounts and fibers, high frequency disturbances.*

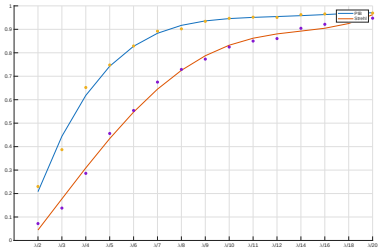

(b) $L_c = 0.5D, \rho = 0.6$. *Substructure modes, mid-frequency bands.*

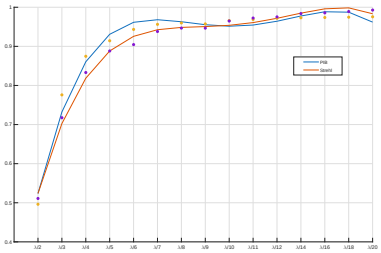

(c) $L_c = 2D, \rho = 0.9$. *Low frequency, global modes.*

Figure 7: *Power-in-the-bucket (PIB) efficiency and Strehl ratio for three different disturbance vibration regimes, with phase noise rms varying from* $\lambda/2$ *to* $\lambda/20$.

When expressed in terms of power-in-the-bucket (PIB), all cases converge toward a common performance ceiling of approximately 97 percent as the phase noise rms decreases, with the threshold of 95 percent PIB consistently reached once the residual error is below about $\lambda/10$. The most detrimental case corresponds to uncorrelated, high-frequency disturbances, which show the slowest recovery in PIB as the noise level is reduced. This behaviour indicates that local, uncorrelated jitter has a stronger impact on the effective energy capture at the receiver than globally correlated or lower-frequency disturbances. In contrast, the Strehl ratio degrades significantly in all regimes, but since the application is power transmission rather than high-resolution imaging, the concentration of energy into the receiver aperture (PIB) is the more relevant metric. These findings suggest that while high-frequency uncorrelated noise should be mitigated as much as possible, the overall tolerance of the system to phase disturbances is acceptable provided the residual rms error can be maintained below $\lambda/10$. Importantly, for wireless power transmission the PIB is the primary figure of merit, since the goal is to maximise the fraction of transmitted energy collected by the receiver, rather than to preserve diffraction-limited beam quality as quantified by the Strehl ratio.

5.3 Beam steering capabilities

In CBC, electronic phase steering demonstrated agile re-pointing of the far-field lobe by several tens of microradians without mechanical motion, effectively retargeting the beam within fractions of a second. In SBC, beam steering must be accomplished through mechanical pointing of the final optical assembly, which is slower and introduces additional mass and complexity. These simulations highlight a **key architectural trade-off**: CBC offers intrinsic electronic steering flexibility but demands precise phase control, while SBC simplifies phase management but relies on conventional pointing mechanisms. Indeed, SBC steering relies on a large mirror or gimbal system to redirect the full coaxial beam. Such assemblies contribute significantly to spacecraft mass and occupy considerable payload volume. They also introduce moving parts, which are potential points of

Copyright 2025 by the authors, Published by the IAF, with permission and released to the IAF to publish in all forms.

failure and require continuous power to actuate. In addition, the mirror's optical coating has finite efficiency, so non-ideal reflectivity or absorption leads to incremental power losses in the whole system. Mechanical steering mechanisms therefore impose penalties in mass, reliability, and optical throughput, which must be balanced against the relative simplicity of CBC phase management.

6. Conclusions

The study assessed the performance of coherent (CBC) and spectral (SBC) beam combining architectures for long-distance laser power transmission. A particular focus was placed on the impact of imperfect phase control and structural vibrations. In CBC, residual phase noise was shown to degrade constructive interference, lowering the on-axis intensity, and redistributing energy into sidelobes. The sensitivity was strongest to uncorrelated, high-frequency jitter that cannot be corrected by feedback loops. In contrast, SBC, which combines fields incoherently, is unaffected by internal phase fluctuations, although misalignment and pointing jitter still broadened the receiver footprint, but in both architectures. This highlights the robustness of SBC to internal coherence errors, at the expense of relying on bulkier optical steering. Beyond phase noise, the architectures were compared in terms of end-to-end transmission efficiency. To ensure a consistent metric, the *power-in-the-bucket* (PIB) efficiency was introduced in place of the geometric efficiency traditionally used for SBC. This allowed direct quantification of the fraction of transmitted power collected by a finite receiver aperture. Results showed that, for comparable transmitter diameters, both CBC and SBC achieve similar diffraction-limited footprints, with efficiency ultimately driven by receiver size and pointing stability rather than the combining method itself. Finally, the analysis highlights the trade-offs between the two approaches: CBC enables electronic beam steering and scalability but demands precise phase control, while SBC avoids coherence sensitivity but requires mechanically steered optics. Looking forward, artificial intelligence methods have shown promise in accelerating stochastic parallel gradient descent (SPGD) algorithms for real-time phase correction, opening pathways to more robust CBC operation in practical scenarios [18], [19]. An experimental campaign will also be useful in the validation of the feasibility of coherent combination and the impact of different types of disturbances.

Acknowledgements

The authors thank ASI for funding the research within the call 'Sviluppo di progetti/esperimenti scientifici per la Luna – Development of project/scientific experiments for the Moon; BANDO ASI n. prot. DC-DSR-UVS-2022-375.

References

[1] Y. R. Z. F. Y. X. Z. X. P. Z. P. L. L. Y. J. J. L. F. G. C. L. X. Liu Jiaying, Li Ziqiang, "Research progress of coherent beam combining technique of phased fiber laser arrays," *High Power Laser and Particle Beams*, 2023. Latest PFLA / phased fiber laser array tech from Chinese Academy of Sciences.

[2] M. S. S. M. S. D. A. V. D. S. B. Linslal Charles Lailabai, Ayyaswamy Padmanabhan, "Challenges in coherent beam combining of high power fiber amplifiers: a review," *ISSS Journal of Micro and Smart Systems*, vol. 11, pp. 277–293, Jun 2022.

[3] L. Y. L. Y. Z. H. C. Q. L. M. S. Q. F. X. H. W. J. F. Yan Yuefang, Tao Rumao, "Research progress and prospect of high power all-fiber coherent beam combination based on fiber combining devices," 2023.

[4] Q. Gao, Z. Li, W. Zhao, G. Li, P. Ju, W. Gao, and W. Dang, "Spectral beam combining of fiber lasers with 32 channels," *Optical Fiber Technology*, vol. 78, p. 103311, 2023.

[5] R.-J. Wang, X.-J. Wang, J. Yang, L. Yuan, Y.-Y. Lin, K. Liu, D.-F. Cui, Y. Kou, Y. Liu, and Q.-J. Peng, "Demonstration of the spectral beam combining in a yb:yag slab laser resonator," *IEEE Journal of Quantum Electronics*, vol. 58, no. 5, pp. 1–6, 2022.

Copyright 2025 by the authors, Published by the IAF, with permission and released to the IAF to publish in all forms.

[6] R. W. B.S. Tan, P.B. Phua, "Spectral beam combining of yb-doped fiber lasers using wavelength dependent polarization rotators and polarization beam combiners," *arXiv (or Optical Letters equivalent)*, 2007. Early experiment of SBC with two Yb lasers, shows combining efficiency and how SBC works in practice.

[7] P. S. I. Authors, "Towards ultimate high-power scaling: Coherent beam combining of fiber amplification channels," *Photonics*, vol. 8, no. 12, p. 566, 2021. Review of CBC in both CW ultrafast fiber lasers, scaling challenges and architectures.

[8] Z. Pu, L. Ze-Jin, W. Xiao-Lin, M. Yan-Xing, L. Xiao, X. Xiao-Jun, and G. Shao-Feng, "Coherent beam combining of three watt-level fiber amplifiers using a dsp-based stochastic parallel gradient descent algorithm," *Chin. Phys. Lett.*, vol. 26, no. 4, pp. 044202–044202, 2009.

[9] M. Björck, M. Henriksson, and L. Sjöqvist, "Outdoor target-in-the-loop coherent beam combination using a stochastic parallel gradient descent algorithm," in *Technologies for Optical Countermeasures XVIII and High-Power Lasers: Technology and Systems, Platforms, Effects V* (D. H. Titterton, R. J. Grasso, M. A. Richardson, W. L. Bohn, and H. Ackermann, eds.), vol. 11867, p. 118670E, International Society for Optics and Photonics, SPIE, 2021.

[10] G. Yang, L. Liu, Z. Jiang, J. Guo, and T. Wang, "Incoherent beam combining based on the momentum spgd algorithm," *Optics Laser Technology*, vol. 101, pp. 372–378, 2018.

[11] H. Zhou, X. Feng, L. Xie, M. Li, H. Zhang, R. Tao, H. Lin, J. Wang, L. Yan, and F. Jing, "Comprehensive investigation of locset and spgd algorithms in coherent beam combining applications," *Optics Laser Technology*, vol. 181, p. 111568, 2025.

[12] J. X. T. H. P. Z. Hongxiang Chang, Qi Chang, "First experimental demonstration of coherent beam combining of more than 100 beams," *Photonics Research*, vol. 8, p. 1943, 2020.

[13] A. Garcia, T. Gust, E. Basata, T. Gersting, M. Deka, S. Thiele, M. Salah, M. Koerner, T. Runte, and M. Gonzalez, "Vibes: Visionary ingenuity boosting european spacecraft. managing microvibrations for the future of spaceflight," *Archive of Mechanical Engineering*, pp. 183–197, 02 2023.

[14] C. Spindeldreier, B. Ustaoglu, U. Kulau, and J. Rust, "Performance evaluation of space-grade fpga architectures," in *2023 European Data Handling Data Processing Conference (EDHPC)*, pp. 1–5, 2023.

[15] S. Qaani and N. Siahvashi, "Optimizing geometrical parameters of coherent beam combining in the near and far-field distance," *Optik*, vol. 296, p. 171536, 2024.

[16] R. Heintzmann, L. Loetgering, and F. Wechsler, "Scalable angular spectrum propagation," *Optica*, vol. 10, pp. 1407–1416, Nov 2023.

[17] E. C. for Space Standardization (ECSS), "Ecss-e-hb-32-26a, spacecraft mechanical loads analysis handbook," 2 2013.

[18] H. Jia, J. Zuo, Q. Bao, C. Geng, X. Li, F. Li, Z. Li, J. Jiang, J. Liu, Y. Xia, F. Zou, X. Yang, J. Jiang, J. Ren, and B. Li, "A phase-error prediction method for coherent beam combining via convolutional neural network," *Optik*, vol. 246, p. 167827, 2021.

[19] C. L. H. C. W. H. L. Y. Yong Wu, Guoqing Pu, "Harnessing artificial intelligence for coherent beam combination," *Optics / Journal placeholder*, 2024. Recent work on AI-assisted phase control in CBC.